Journal of Coastal Research	36	2	424–433	Coconut Creek, Florida	March 2020

www.JCRonline.org

TECHNICAL COMMUNICATIONS

www.cerf-jcr.org

Pitch Angle Control with Model Compensation Based on Active Disturbance Rejection Controller for Underwater Gliders

Tingting Guo[†], Dalei Song[†]*, Kunqian Li[†], Chong Li[†], and Hua Yang[‡]

[†]College of Engineering
Ocean University of China
Qingdao 266100, China

[‡]College of Information Science and Engineering
Ocean University of China
Qingdao 266100, China

ABSTRACT

Guo, T.; Song, D.; Li, K.; Li, C., and Yang, H., 2020. Pitch angle control with model compensation based on active disturbance rejection controller for underwater gliders. *Journal of Coastal Research,* 36(2), 424–433. Coconut Creek (Florida), ISSN 0749-0208.

As the pitch angle control system of an underwater glider is nonlinear, multivariate, and has strong coupling, active disturbance rejection control (ADRC) was applied in the pitch angle control loop. To improve the control precision and responsiveness, a model compensation (MC) was presented to alleviate the estimation pressures for the extended state observer in the ADRC. The vast majority of parameters in the MC were estimated and identified so that the ADRC controller can work better. Simulation experiments illustrated that the MC based on ADRC was effective. For the pitch angle control, the overshoot was reduced by 4.5% and the settling time dropped to 90 seconds compared with the traditional ADRC. It demonstrated a more accurate motion trajectory control effect for an underwater glider. Besides, the MC-ADRC controller has better dynamic characteristics and antidisturbance ability, which ensure that the underwater glider is more anti-interference and flexible.

ADDITIONAL INDEX WORDS: *Active disturbance rejection control, parameter identification.*

INTRODUCTION

An autonomous underwater glider (AUG) is a kind of autonomous underwater vehicle without external propulsion (Caffaz *et al*., 2009; Carneiro and Almeida, 2018). It relies on the balance between buoyancy and hydrodynamic forces. By changing the buoyancy through the buoyancy adjustment mechanism, a glider can be descending and ascending with sawtooth trajectories (Liu *et al*., 2018; Mahmoudian and Woolsey, 2009). Its mechanical structure determines its many advantages such as low electric consumption as well as super-long voyage capability (Leonard *et al*., 2007; Yoon and Kim, 2017). The most famous gliders include *Slocum* (Glenn *et al*., 2011), *Seaglider* (Eriksen *et al*., 2001), *Spray* (Sherman *et al*., 2001), and *Petrel* (Wang *et al*., 2010).

In an AUG system, the ballast tank, which is configured in the head of the glider, is used to adjust buoyancy for gliders to float and dive (Claus, Bachmayer, and Cooney, 2012). A sliding battery pack is used for pitch angle control (Afande, Arshad, and Mohd-Mokhtar, 2011; Leonard *et al*., 2007). The zigzag motion trajectory determines that the pitch angle control is very important for gliders (Leonard *et al*., 2007). However, the ballast tank is not coincident in the buoyancy center, so it would have a serious impact on pitch angle (Leonard and Graver, 2001). Furthermore, the pitch angle is always affected by many other factors, such as the glider motion velocity and external sea currents under the water (Shih *et al*., 2016; Song *et al*., 2018).

To solve the control problem of pitch angle, some algorithms were proposed, such as the linear quadratic regulator (LQR) (Isa and Arshad, 2013; Tchilian *et al*., 2017) and the fuzzy proportional integral derivative method (fuzzy PID) (Noh, Arshad, and Mokhtar, 2011). Fuzzy PID performed better than the LQR algorithm in terms of control precision (Cao *et al*., 2015). However, most of these previous works are based on the linear control equations. The performances of these controllers are weak, even invalid when the system state departs from the equilibrium point, and are sensitive to parameter perturbations and external disturbances (Afande, Arshad, and Mohd-Mokhtar, 2011).

Active disturbance rejection control (ADRC) is a powerful control technique for coupling and nonlinear systems (Gao, 2006) that was proposed by Han (Han, 2009; Sun, 2007; Zheng, Chen, and Gao, 2009). ADRC avoids large overshoot by arranging the transition process through a tracking differentiator (TD) and enhancing robustness. The system uncertainties and total disturbances were observed by the extended state observer (ESO). By means of designing the nonlinear state error feedback (NLSEF) and combing the observation of ESO for the system status and unknown disturbance, the linearization of the dynamic compensation is sequentially

DOI: 10.2112/JCOASTRES-D-19-00050.1 received 12 April 2019; accepted in revision 14 July 2019; corrected proofs received 31 October 2019.

*Corresponding author: songdalei@ouc.edu.cn

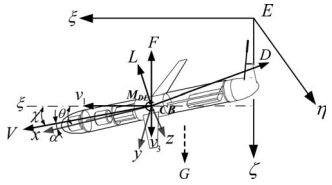

Figure 1. Coordinate definition and force diagram for a glider. This figure describes three coordinate frames and directions of some vectors and variables for an underwater glider.

realized. The most significant advantage of ADRC is that it does not need any mathematical models of the controlled object (Su *et al*., 2004; Sun, 2007; Xue and Huang, 2014).

Since many factors influence pitch angle, such as battery pack position, volume of the ballast tank, velocity, ocean currents, *etc*., ADRC is difficult to use for good performance of gliders. These factors vary during the gliding motion, which means that both of these perturbation terms and disturbances are time variant. Obviously, it is a heavy burden for ESO to estimate these perturbation terms and disturbances.

To solve this problem, a model compensation (MC) based on the ADRC was proposed in this paper and called MC-ADRC. Via estimating parameters for the compensation model, the ESO does not need to estimate the whole disturbance, only those that are not compensated. In addition, a parameter identification method was presented to obtain more precise parameters for the compensation model. Other parameters in the compensation model can be obtained through estimating or physical sensors. The ESO estimation pressures are significantly reduced and the MC-ADRC performs with higher control precision and stronger anti-interference abilities for an underwater glider.

METHODS

This section describes the work of establishing the kinetic equations for the glider, and the MC algorithm based on the ADRC.

Coordinate Frame Definition

The classical kinetic model was proposed by Graver (2005). It assumed that the ballast tank was coincident with the buoyancy center. On the basis of the modeling approach from the literature (Graver, 2005; Schofield *et al*., 2007), the kinetic equations are derived, which indicates that the ballast tank is inconsistent with the buoyancy center for a glider (Leonard *et al*., 2007).

The coordinate frame for the glider is shown in Figure 1: an inertial frame $E-\xi\eta\zeta$ with the $E\zeta$ direction toward Earth's center and the $E\xi$ axis parallel to the horizontal plane and pointing to the head of the glider; and a body frame $O-xyz$ lies on the glider body with the origin at the buoyancy center. The Ox axis points to the head of the glider. The Oy axis parallels with the horizontal wing and is perpendicular to the Ox axis. The Oz axis is perpendicular to Ox and Oy.

The position of the glider $b=(x,y,z)$ is the vector from the origin of the inertial coordinate to the origin of the body coordinate. The vector orientation is given by a rotation matrix $\mathbf{R}$ depicted by the Euler angles yaw, pitch, and roll. The glider's velocity and angular rate in the body frame are denoted as $\mathbf{V}=[v_1,v_2,v_3]^T$ and $\Omega=[\Omega_1,\Omega_2,\Omega_3]^T$.

Mathematical Model with Kinetic Equations

Under an equilibrium state, the glider is balanced with gravity G, buoyancy F, water resistance D, lift force L, and viscous moment M_{DL}. In the vertical plane, the glider moves with translational velocity $(v_1,0,v_3)$ relative to the inertial coordinate. The glider motion variables are shown as follows:

$$R=\begin{bmatrix}\cos\theta & 0 & -\sin\theta\\ 0 & 1 & 0\\ \sin\theta & 0 & \cos\theta\end{bmatrix},\mathrm{b}=\begin{bmatrix}x\\0\\z\end{bmatrix},V=\begin{bmatrix}v_1\\0\\v_3\end{bmatrix},\Omega=\begin{bmatrix}0\\\Omega_2\\0\end{bmatrix},r_p=\begin{bmatrix}r_{p1}\\0\\\mathrm{const}\end{bmatrix},P_p=\begin{bmatrix}P_{p1}\\0\\P_{p3}\end{bmatrix},U_p=\begin{bmatrix}u_{p1}\\0\\0\end{bmatrix},r_b=\begin{bmatrix}\mathrm{const}\\0\\0\end{bmatrix},P_b=\begin{bmatrix}P_{p1}\\0\\P_{b3}\end{bmatrix}.$$

R is the rotation vector between the inertial coordinate and body coordinate. $V=\sqrt{{v_1}^2+{v_3}^2}$ is the velocity and Ω denotes the pitch angle. The battery packs have only one degree of freedom along with the x axis and its position vector is $r_{p3}=0$. For the buoyancy adjustment mechanism, $r_{b1}=\mathrm{const}$ and $r_{b3}=0$. u_{p1} is the input. From these constraint terms, the vertical motion equations can be simplified as follows:

$$\dot{x}=v_1\cos\theta+v_3\sin\theta \tag{1}$$

$$\dot{z}=v_1\sin\theta+v_3\cos\theta \tag{2}$$

$$\dot{\theta}=\Omega_2 \tag{3}$$

$$\dot{\Omega}_2=\frac{1}{J_2}[(m_3-m_1)v_1v_3-(r_{p1}P_{p1}+r_{p3}P_{p3})\dot{\theta}-r_{b1}P_{b1}\dot{\theta}-m_pg(r_{p1}\cos\theta+r_{p3}\sin\theta)-m_bgr_{b1}\cos\theta+M_{\mathrm{DL}}-r_{p3}u_{p1}] \tag{4}$$

$$\dot{v}_1=\frac{1}{m_1}\left[-m_3v_3\Omega_2-P_{p3}\Omega_2-m_0g\sin\theta+L\sin\alpha-D\cos\alpha-u_{p1}\right] \tag{5}$$

$$\dot{v}_3=\frac{1}{m_1}\left[m_1v_1\Omega_2+P_{p3}\Omega_2+P_{b1}\Omega_2+m_0g\cos\theta-L\cos\alpha-D\sin\alpha\right] \tag{6}$$

$$\dot{r}_{p1}=\frac{1}{m_p}P_{p1}-v_1-r_{p3}\Omega_2 \tag{7}$$

$$\dot{r}_{p3}=\frac{1}{m_p}P_{p3}-v_3+r_{p1}\Omega_2 \tag{8}$$

$$\dot{P}_{p1}=u_{p1} \tag{9}$$

Table 1. *Definitions for some variables with the glider.*

Name	Description	Name	Description
m_i	ith diagonal element of M	m_0	Excess mass
P_p	Linear moment of m_p in body coordinates	P_b	Linear moment of m_b in body coordinates
C_D	Standard aerodynamic drag coefficients by A	C_L	Standard aerodynamic lift coefficients by A
C_M	Standard aerodynamic moment coefficients by A	A	Maximum glider cross-sectional area
ρ	Fluid density	r_p	m_p position in body coordinates
r_b	m_b position in body coordinates		

α is the angle of attack (AOA). It is the angle between the body x axis and the velocity V (Font *et al.*, 2012). χ is the path angle with $\chi = \theta - \alpha$.

$$D = \frac{1}{2}\rho C_D(\alpha)AV^2 = (K_{D0} + K_D\alpha^2)\cdot(v_1{}^2 + v_3{}^2) \tag{10}$$

$$L = \frac{1}{2}\rho C_L(\alpha)AV^2 = (K_{L0} + K_L\alpha)\cdot(v_1{}^2 + v_3{}^2) \tag{11}$$

$$M_{DL} = \frac{1}{2}\rho C_M(\alpha)AV^2 = (K_{M0} + K_M\alpha)\cdot(v_1{}^2 + v_3{}^2) \tag{12}$$

C_D, C_L, and C_M are the functions of α and Ks are constant coefficients. K_{D0}, K_{L0}, K_{M0}, K_D, K_L, and K_M are hydrodynamic parameters. Other parameters in the glider kinetic model are given in Table 1.

According to the equation $\ddot{\theta} = \dot{\Omega}_2$, the pitch angle control equation can be formulated as follows:

$$\ddot{\theta} = \frac{1}{J_2}[(m_3 - m_1)v_1v_3 - (r_{p1}P_{p1} + r_{p3}P_{p3})\dot{\theta} - r_{b1}P_{b1}\dot{\theta} - m_pg(r_{p1}\cos\theta + r_{p3}\sin\theta) - m_bgr_{b1}\cos\theta + M_{DL} - r_{p3}u_{p1}] \tag{13}$$

The general and optimal pitch angles of the glider range from –30° to +30° (Isa and Arshad, 2013). Considering the overshoot of the adjustment, $\sin\theta$ and $\cos\theta$ are unfolded ranges from –40° to 0° (descend phase) and 0° to +40° (ascend phase) according to the Taylor formula $\sin\theta \approx a_1 + b_1\theta + c_1\theta^2$ and $\cos\theta \approx a_2 + b_2\theta + c_2\theta^2$, where a, b, and c are the coefficients of the fitting curves (Table 2).

Eliminating the high-order terms, it is transformed as a standard equation $\ddot{\theta} = f(\theta, \dot{\theta}, w) + bu$, where w is the disturbances and $u = f(u_{p1})$ are the input variables and parameter b is the coefficient.

$$\ddot{\theta} = \frac{1}{J_2}\begin{Bmatrix} -(r_{p1}P_{p1} + r_{p3}P_{p3} + r_{b1}P_{b1})\dot{\theta} - (b_2m_pg + \mathrm{b_1}m_pgr_{p3} + b_2m_bgr_{b1})\theta \\ -(a_2m_pgr_{p1} + a_1m_pgr_{p3} + a_2m_bgr_{b1}) + (m_3 - m_1)v_1v_3 + M_{DL} - r_{p3}u_{p1} \end{Bmatrix} \tag{14}$$

It is obvious that the pitch angle control system is nonlinear. It is influenced by the battery pack position r_p and oil sac volume m_b. In addition, it is also influenced by the velocity V, viscous moment M_{DL}, and external disturbances such as ocean currents in practical applications.

ADRC Algorithm

ADRC adopted the kernel of the classic PID controller in which adjustment is based on the feedback error. From the reference of state observation theory, it constructs a new controller by nonlinear combinations. Furthermore, ADRC has overcome the weakness of the traditional PID controller, which cannot obtain differential signals. Substantially, the ADRC algorithm tracks input and differential signals by TD. Moreover, it tracks output and differential signals by ESO. The core idea of ADRC is that it estimates and compensates on the basis of attributing unmodeled dynamics and unknown external disturbances to "overall disturbances" (Han, 2009). The structure of the ADRC is shown in Figure 2.

In the pitch angle control system for the glider, the system additive perturbation and the external disturbances are attributed to the general disturbance. The ESO estimates the general perturbation and compensates in the form of the feedforward.

Considering two-order nonlinear object:

$$\begin{cases} \ddot{x} = f(x, \dot{x}) + w(t) + bu(t) \\ y = x(t) \end{cases} \tag{15}$$

First, the TD has the function of extracting the continuous signal and its differential signal. The input signal is $v_0(t)$ and output signals are $v_1(t)$ and $v_2(t)$. Signal $v_1(t)$ tracks the signal $v_0(t)$ and $v_2 = \dot{v}_1$. In other words, signal $v_2(t)$ is the "approximate differential" for signal $v_0(t)$.

$$\begin{cases} e = v_1 - v_0 \\ \dot{v}_1 = v_2 \\ \dot{v}_2 = f_{\mathrm{han}}(e, v_2, r_0, h_0) \end{cases} \tag{16}$$

In Equation (16), r_0 denotes the speed factor, h_0 is the filter factor, and f_{han} represents the optimal control function, which is defined as follows:

$$f_{\mathrm{han}}(e, v, r, h) = \{ -r\mathrm{sign}(a), \quad |a| > d - ra/d, \quad |a| \le d \tag{17}$$

where, $d = rh$, $d_0 = hd$, $y = e + hv$, $a_0 = \sqrt{d^2 + 8r|y|}$.

$$a = \{ v + \mathrm{sign}(y)(a_0 - d)/2, \quad |y| > d_0v + y/h, \quad |y| \le d_0 \tag{18}$$

Second, the ESO is designed as follows:

$$\begin{cases} e = z_1 - x \\ \dot{z}_1 = z_2 - \beta_{01}e \\ \dot{z}_2 = z_3 - \beta_{02}f_{al}(e, 0.5, h) + b_0u \\ \dot{z}_3 = -\beta_{03}f_{al}(e, 0.25, h) \end{cases} \tag{19}$$

Parameter u is the input variable. z_1 is the estimation of output state variable and z_2 is the speed estimation of output. h represents the sampling step, and β_{01}, β_{02}, and β_{03} are the controller parameters. Nonlinear function f_{al} is defined by the following equation:

$$f_{\mathrm{al}}(e, \alpha, \delta) = \begin{cases} e/\delta^{1-\alpha}, & |e| \le \delta \\ |e|\alpha\mathrm{sign}(e), & |e| > \delta \end{cases} \tag{20}$$

Each state tracks its status variable that was extended: $z_1(t) \to x(t)$, $z_2(t) \to \dot{x}(t)$, $z_3(t) \to \ddot{x}(t) \to f(x, \dot{x}, w)$.

Table 2. *Coefficients of the fitting curves for functions* $\sin\theta$ *and* $\cos\theta$.

	$\sin\theta$			$\cos\theta$		
Angle Range	a_1	b_1	c_1	a_2	b_2	c_2
(−40°, 0°)	−0.011	0.0162	0	1.0008	2.205E-4	−1.418E-4
(0°, +40°)	0.011	0.0162	0	1.0008	2.205E-4	−1.418E-4

Third, the traditioinal PID algortihm uses the weighted sum form through the error proportion, differential, and integral (Rivera, Morari, and Skogestad,1986). However, it is unfavorable for solving the contradiction between speed and the overshoot. NLSEF makes good use of the past, present, and future informatioin for error. In ADRC, the state estimation output z_i from ESO is assumed as the state feedback variable. It was compared with the output v_i from TD. The error amount $e_i = v_i - z_i$ constitutes the nonlinear combination for system error feedback.

$$\begin{cases} e_1 = v_1 - z_1 \\ e_2 = v_2 - z_2 \\ u_0 = \beta_{11} f_{\text{al}}(e_1, 0.5, h_1) + \beta_{12} f_{\text{al}}(e_2, 1.5, h_1) \end{cases} \tag{21}$$

Parameter β_{11} and β_{12} are gain coefficients.

Last, the disturbance compensation can be donoted as:

$$u = u_0 - z_3/b_0 \tag{22}$$

where, b_0 is the compensation coefficient.

The compensation coefficient b_0 will ensure timely disturbance compensation for the system. Moreover, the disturbance can be observed by the ESO simultaneously. In that case, despite the disturbance, the controller remains at a good control level.

MC Principle Based on ADRC

ADRC is a control method that doesn't depend on the model of the controlled object. It is only related to the control coefficient b. However, the ADRC can make full use of the model information and decrease the estimators for uncertainties by importing the MC. The MC reduces the estimation errors for ESO, and it improves the dynamic control performances.

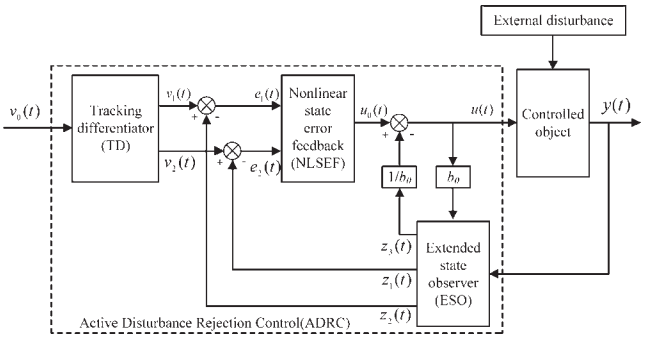

Figure 2. Structure of ADRC. It includes three parts: the TD for arranging the transition process, the ESO for estimating the object, and the NLSEF for nonlinear control.

From the structure of ADRC, the state estimation of the third-order ESO is used for estimating both of the parameter changes of the model and the external disturbances. However, when the object model changes acutely or the external disturbances are oversized, the ESO must have a good tracking performance. In particular, the parameter z_3 must have a very high estimation precision when the desired output changes acutely or the disturbances are oversized. In other words, the approach to improving tracking performance for ESO reduces the estimation errors of z_3 as much as possible. That means that the observed pressure of the ESO from the uncertainties would be reduced substantially by means of substituting the known model parameters into the observation function.

Suppose that $f(x,\dot{x}) = f_1(x,\dot{x}) + f_2(x,\dot{x})$, where $f_1(\cdot)$ and $f_2(\cdot)$ denote the known and unknown model respectively. On the basis of the ESO, let $x_3 = f_2(x,\dot{x},w)$, so $z_3 \to f_2(x,\dot{x},\cdots,x^{(n-1)},t) + w(t)$. The ESO observation equation became the following:

$$\begin{cases} \dot{z}_1 = z_2 - \beta_{01} e \\ \dot{z}_2 = z_3 - \beta_{02} f_{al}(e, 0.5, h) + f_1(x,\dot{x}) + b_0 u \\ \dot{z}_3 = -\beta_{03} f_{al}(e, 0.25, h) \end{cases} \tag{23}$$

The system was approximated as the "integrator series model." The feedback compensation is $u(t) = u_0(t) - [z_3 + f_1(x,\dot{x})]/b$.

In the conventional ESO along with the AUG system, z_3 is the estimation value for external disturbances and contains many dynamic estimation, measurement, and identification missions including θ, $\dot{\theta}$, r_p, m_b, v_1, v_3, and M_{DL}.

It can be seen that the system has proposed exorbitant requirements for ESO when the parameters m_b, θ, V, and M_{DL} change tempestuously. In other words, z_3 must possess strong tracking and observation abilities.

Rewriting the pitch angle control equation as follows:

$$\ddot{\theta} = f_1(\theta,\dot{\theta}) + f_2(\theta,\dot{\theta},w) + bu \tag{24}$$

$f_1(\theta,\dot{\theta})$ is the given model that can be estimated and $f_2(\theta,\dot{\theta},w)$ is the unknown model.

The ESO estimation equation can be written as $z_3 = f_2(\theta,\dot{\theta},w) + (b - b_0)u$. Toward the control equation, the input is: $bu = -r_{p3}u_{p1}$.

According to the structural characteristics of the underwater glider, parameters θ and $\dot{\theta}$ can be measured by the micro-inertial measurement unit named MTi sensor. Battery pack position r_{p1} can be measured by the film potentiometer. Because of α, the horizontal component v_1 and vertical component v_3 of the velocity V cannot be obtained according to the pitch angle θ. It is essential to estimate parameter α according to the known variables. Furthermore, C_D, C_L, and C_M are the functions of α. All these parameters can be obtained by the hydrodynamics identification.

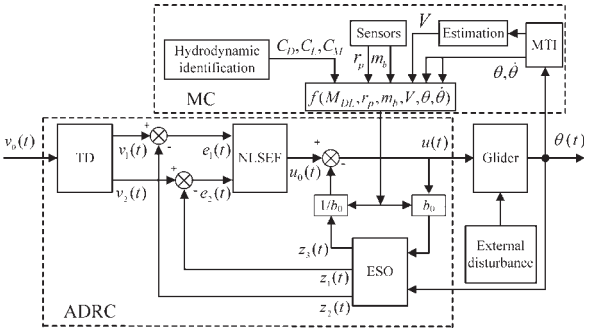

Figure 3. Pitch angle control based on MC-ADRC for the glider diagram. On the basis of ADRC, the model compensation is added for estimating the unknown disturbances.

For glider kinetic equations, function $f_1(\theta,\dot{\theta},w) = -(r_{p1}P_{p1} + r_{p3}P_{p3})\dot{\theta} - (b_2 m_p g + \mathrm{b}_1 m_p g r_{p3})\theta - (a_2 m_p g r_{p1} + a_1 m_p g r_{p3})$ is clear, and the unknown model is:

$$f_2(\theta,\dot{\theta},w) = -r_{b1}P_{b1}\dot{\theta} - b_2 m_b g r_{b1}\theta - a_2 m_b g r_{b1} + (m_3 - m_1)v_1 v_3 + M_{DL} \tag{25}$$

On the basis of the ESO, the estimator is equal to zero if these four conditions are established: (1) Parameter z_1 could track pitch angle θ commendably. (2) m_b can be measured accurately. (3) Velocity v_1 and v_3 could be estimated precisely on the basis of the pitch angle θ. (4) Hydrodynamic parameter M_{DL} can be identified precisely. (5) b=b_0. Certainly, the conditions above are so restricted, even if $b \neq b_0$ or there are some estimate errors in the (1)–(4), what is left of z_3 that needs to be estimated is only $(b-b_0)u$, which is much smaller than before. The observation burden and the disturbances of ESO have been reduced greatly so that it could have a great improvement for estimation precision.

The diagram of pitch angle control based on MC-ADRC for a glider is shown in Figure 3.

Parameters Estimation for MC-ADRC for α with V

The external appearance of the glider is asymmetric in the vertical direction. The α always exists for the sake of the hydrodynamic coefficients. It is easy to obtain the pitch angle of the underwater glider by the physical sensor. However, the precise motion angle of the velocity is unknown; in that case, it is difficult to acquire the AOA (α) between the body x axis and the direction of the motion velocity V.

The method for calculating velocity V is as follows: obtain the vertical velocity component v_3 through the depth pressure sensor. $\chi \approx \theta$ can be established by supposing that α is small enough. In that case, the horizontal velocity component $v_1 \approx v_3$. So, assume that $V \approx V'$ in Figure 4. In fact, this assumption is not exactly right as α is not equal to zero, and it is time variant.

When motion of a glider is stable, the torque equilibrium equation can be obtained according to the kinetic equation of the glider:

$$F_B - F_G - \frac{\rho A_D V^2}{2}(C_{D0} + C_{D1}\alpha^2)\frac{\sin^2\chi + \cos^2\chi}{\sin\chi} = 0 \tag{26}$$

C_{D0} and C_{D1} are the coefficients and determine the total (*i.e.* sum of drag from both the hull and the wings) parasite drag and induced drag, respectively. The quantity A_D is the wing surface area; V is the glider velocity through water along the glider path; and F_G is the force due to gravity, where m is the mass of the glider and g is the acceleration due to gravity. The net buoyancy force is defined as F_B.

The expression of α becomes $\alpha = \frac{C_{D0}+C_{D1}\alpha^2}{(a_w+a_h)\tan(\theta+\alpha)}$, where a_h and a_w are the lift-slope coefficients for the hull and wings, respectively.

It can be seen that the α is only related to the pitch angle θ. That means that it easily gets the accurate velocity V through the pitch angle θ, which is measured by the high-precision MTi sensor. In that case, the velocity disturbance in the ESO would be eliminated consequently.

Parameter Identification for M_{DL}

Suppose the left sides of the kinetic Equations (5) and (6) are equal to zero; the stable equilibrium equations for a glider are as follows:

$$0 = -m_{0_{\mathrm{eq}}} g \sin\theta_{\mathrm{eq}} + L_{\mathrm{eq}} \sin\alpha_{\mathrm{eq}} - D_{\mathrm{eq}} \cos\alpha_{\mathrm{eq}} \tag{27}$$

$$0 = m_{0_{\mathrm{eq}}} g \cos\theta_{\mathrm{eq}} - L_{\mathrm{eq}} \cos\alpha_{\mathrm{eq}} - D_{\mathrm{eq}} \sin\alpha_{\mathrm{eq}} \tag{28}$$

When the glider motions have been in steady state, the lift force and drag force satisfy

$$\chi_{\mathrm{eq}} = -\tan^{-1}\left(\frac{D_{\mathrm{eq}}}{L_{\mathrm{eq}}}\right) \tag{29}$$

The relationship between depth and velocity is as follows:

$$V = \left|\frac{\dot{z}}{\sin(\theta-\alpha)}\right| \tag{30}$$

Putting Equations (10)–(12) and (16) into the equilibrium state Equations (27) and (28).

$$\frac{1}{2}\rho C_L(\alpha_{\mathrm{eq}})A\left(\frac{\dot{z}_{\mathrm{eq}}}{\sin(\theta_{\mathrm{eq}}-\alpha_{\mathrm{eq}})}\right)^2 \sin\alpha_{\mathrm{eq}} - \frac{1}{2}\rho C_D(\alpha_{\mathrm{eq}})A\left(\frac{\dot{z}_{\mathrm{eq}}}{\sin(\theta_{\mathrm{eq}}-\alpha_{\mathrm{eq}})}\right)^2 \cos\alpha_{\mathrm{eq}} - m_{0_{\mathrm{eq}}} g \sin\theta_{\mathrm{eq}} = 0 \tag{31}$$

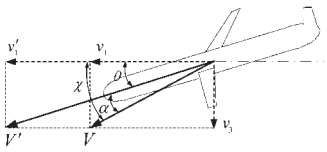

Figure 4. AOA and velocity decomposition in the vertical plane. Velocity V can be decomposed as v_3 in the vertical and v_1 in the horizontal. Velocity V' can be decomposed as v_3 in the vertical and v_1' in the horizontal.

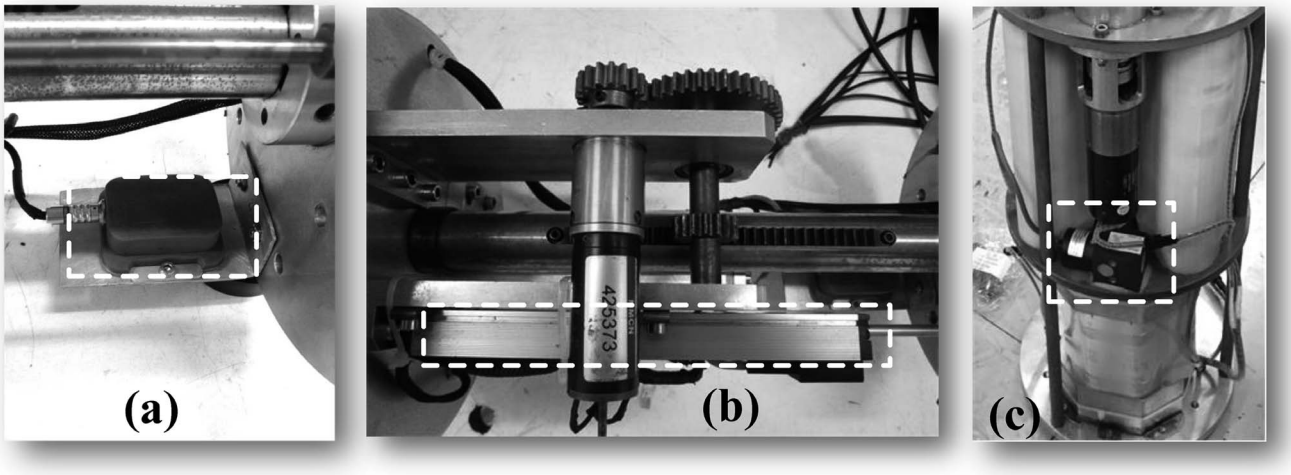

Figure 5. Inertial sensors. (a) MTi. (b) ThinPot film potentiometer. (c) Cable displacement sensor.

$$\frac{1}{2}\rho C_L(\alpha_{\text{eq}})A\left(\frac{\dot{z}_{\text{eq}}}{\sin(\theta_{\text{eq}}-\alpha_{\text{eq}})}\right)^2\cos\alpha_{\text{eq}} - \frac{1}{2}\rho C_D(\alpha_{\text{eq}})A\left(\frac{\dot{z}_{\text{eq}}}{\sin(\theta_{\text{eq}}-\alpha_{\text{eq}})}\right)^2\sin\alpha_{\text{eq}} - m_{0_{\text{eq}}}g\cos\theta_{\text{eq}} = 0 \tag{32}$$

This paper uses a standard $k-\omega$ turbulence calculation model to solve the hydrodynamic parameters (Wilcox, 2008). According to the calculation results, the lift coefficient $C_L(\alpha)$ and α can be fitted by the least-square method: $C_L(\alpha) = 15.234\alpha - 0.0079$.

Similar methods can be used to obtain the drag coefficient $C_D(\alpha)$ and $C_M(\alpha)$:

$$C_D(\alpha) = 65.245\alpha^2 + 0.3893 \text{ and } C_M(\alpha) = 2.434\alpha.$$

In this case, the viscous moment M_{DL} was identified indirectly. The observation burdens of the ESO were further reduced.

Parameter Measurements for θ, $\dot{\theta}$, r_p, and m_b

Pith angle θ can be measured by the MTi sensor in Figure 5(a). The sensor model MTi-10 is designed by the Xsens Company. It is a miniature, gyro-enhanced attitude and heading reference system. Its internal low-power signal processor provides drift-free three-dimensional (3D) orientation as well as calibrated 3D acceleration, 3D rate of turn (rate gyro), and 3D earth magnetic field data. The controller can obtain the pitch angle θ from the MTi sensor in an easy way with a high sampling frequency (10 kHz) and low dynamic error (less than 0.3° in pitch direction), which satisfies the control requirements.

In addition, the pitch angular velocity is the differential signal of pitch angle θ, which is defined as $\dot{\theta} = \frac{d\theta}{dt}$.

Battery pack position r_{p1} can be measured by the ThinPot film potentiometer in Figure 5(b). The ThinPot is a three-wire system with two resistive output channels and an electrical collector channel. By pressing a wiper down onto the top circuit, the ThinPot can produce the desired electrical output. The battery packs are fixed at the sliding rail with the servomotor. The motor drives battery packs and film potentiometer shuttles back and forth. In this way, the position signals r_{p1} of the battery packs could be obtained precisely. In addition, the precision of the ThinPot sensor is 0.5 mm and it meets the requirement.

The glider buoyancy adjustment mechanism is divided into an external oil sac and the internal oil storage tank. In the deep ocean, the shape of the external oil sac is unpredictable and difficult to estimate. However, the internal oil storage tank was designed as the inerratic bellows structure and it carries a cable displacement sensor VXY30 in Figure 5(c). The linear precision of the VXY30 sensor is 0.05% Full Scale (FS) and the transformed buoyancy adjustment precision is 2 mL, which fully meet system requirements.

The cable displacement sensor captures a variable quantity when the net buoyancy m_b changes.

RESULTS

In this section, some pitch angle control and spiral motion experiments were carried out to verify the effectiveness of the proposed algorithm.

Pitch Angle Experiments

For testing the MC-ADRC algorithm, six groups of comparison experiments were simulated and analysed on the MATLAB platform. The adjusting processes were contrasted with the traditional ADRC method.

The parameters of the ADRC r_0, h_0, β_{01}, β_{02}, β_{03}, and h_1 are related to the sampling step length. They can be determined as follows: $r_0 = 0.001/h^2$, $h_0 = 5h$, $\beta_{01} = 1/h$, $\beta_{02} = 1/(3h^2)$, $\beta_{03} = 1/(32h^3)$, $h_1 = 10h$ (Gao, 2006). In addition, gain coefficients β_{11} and β_{12} are equal to the proportional differential gains of PID controller; compensation coefficient b_0 corre-

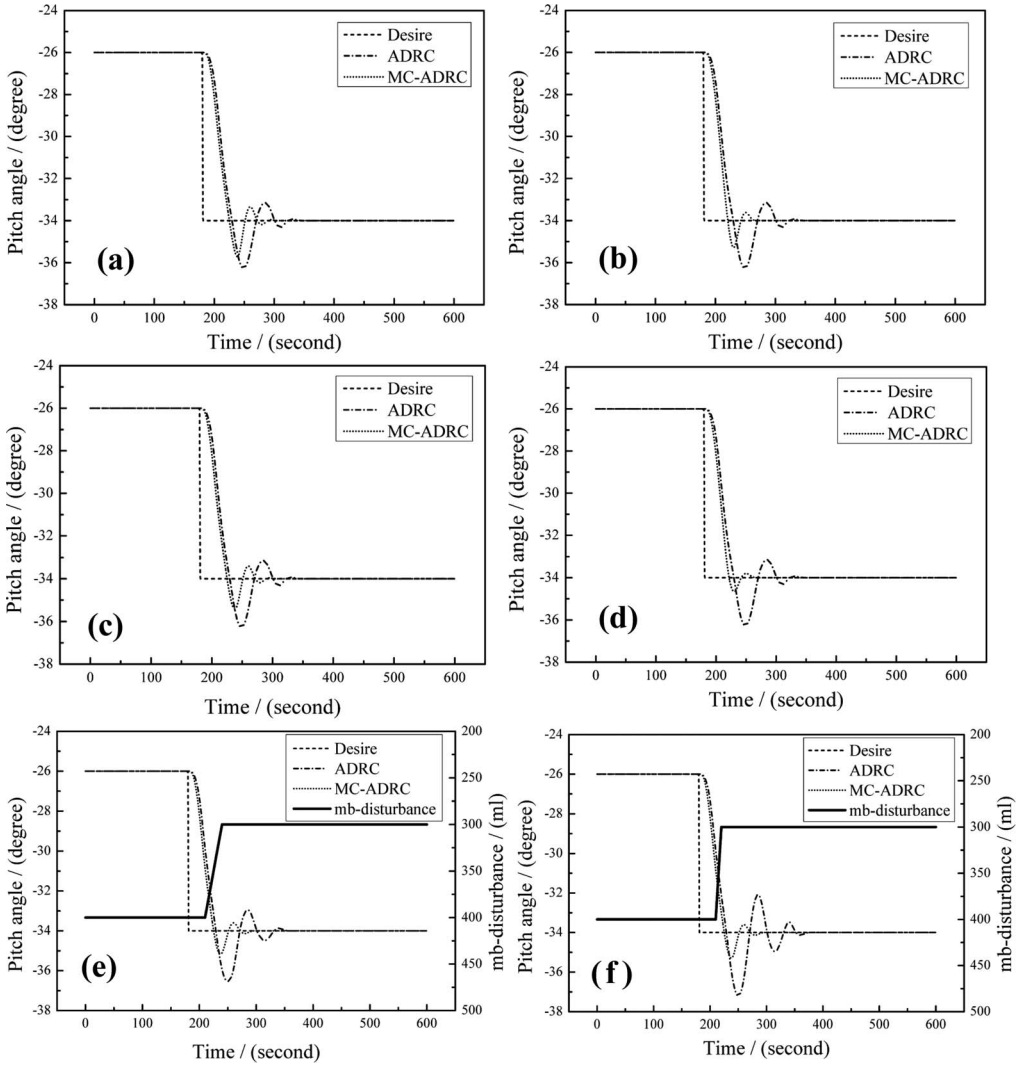

Figure 6. Pitch angle control simulation results with ADRC and MC-ADRC. (a) Experiment I. (b) Experiment II. (c) Experiment III. (d) Experiment IV. (e) Experiment V. (f) Experiment VI.

sponds to the integral gain. Combining the simulation experiences, $\beta_{11} = 2$, $\beta_{12} = 0.9$, and $b_0 = 0.4$.

The control conditions for these six comparison experiments are as follows: stabilizing the glider at a certain velocity V but changing its battery pack position r_{p1} independently, and observing the results and regulation processes of the pitch angle θ between ADRC and MC-ADRC. The initial pitch angle was set at a –26° level, which is most economical, and the desired pitch angle was at –34°. The ADRC and MC-ADRC intervened at 180 seconds in the five control processes below. The disturbance of the variable buoyancy occurs at 190 seconds.

The comparison results are presented in Figure 6. There exists an obvious overshoot in the pitch angle control process. The performances of the MC-ADRC are much better than the ADRC for these six contrast experiments, no matter for the settling time or the overshoot.

For experiment I in Figure 6(a), the ADRC algorithm has no MCs, neither α(as well as the v), nor buoyancy m_b, nor viscous moment M_{DL}. The settling time was up to 155 seconds and the overshoot was more than 6.7%. For the MC-ADRC, the parameter α was estimated accurately in compensation model but the parameters m_b and M_{DL} were not compensated. The settling time was 112 seconds and the overshoot was 5.2%.

Regarding experiment II in Figure 6(b), the ADRC algorithm has no MC and the parameter m_b was compensated in MC-ADRC; the performance comparisons of MC-ADRC and ADRC were 80 seconds *vs.* 155 seconds and 3.5% *vs.* 6.7%.

For experiment III in Figure 6(c), the ADRC algorithm has no model compensation, and the parameter M_{DL} was compensated in MC-ADRC. Obviously, MC-ADRC has a better performance than ADRC and the settling time and overshoot were reduced to 90 seconds and 4.0% in the test, respectively.

Table 3. *Control performance comparisons between ADRC and MC-ADRC.*

	Pitch Angle Control Performances		End-Point Coordinates of 3D Trajectory		
Experiments	M_P/%	t_s/s	X/m	Y/m	Z/m
Desire	0	0	187.6	171.9	−889.3
ADRC	7.5	156	46.6	435.0	−1158.0
MC-ADRC (I)	5.2	112	147.9	368.5	−1080.0
MC-ADRC (II)	3.5	80	141.9	374.1	−1041.4
MC-ADRC (III)	4.0	90	178.0	309.5	−1022.0
MC-ADRC (IV)	2.0	70	182.0	171.0	−897.5
MC-ADRC (V)	3.3	95	167.1	329.5	−946.0
MC-ADRC (VI)	3.8	101	130.0	383.1	−984.1

For experiment IV with disturbance in Figure 6(d), the ADRC algorithm similarly has no MC and the MC-ADRC parameters m_b, M_{DL}, and α were estimated accurately. The performance differences were even greater. MC-ADRC has a shorter settling time of 90 seconds and a small overshoot of 4.0%. However, the ADRC has a large overshoot process, the settling time was up to 165 seconds, and the overshoot reached 6.7%.

For experiment V, the ADRC algorithm has no MCs, neither α, nor m_b, nor M_{DL}. However, all of the parameters, including m_b, M_{DL}, and α, were estimated precisely in MC-ADRC. In this test, a disturbance in the adjustment process was added for pitch angle from 210 seconds to 240 seconds. More specifically, the buoyancy changed from 400 mL to 300 mL slowly when the pitch angle changed from –26° to –34°. In that case, the control process encountered was an andante disturbance. The result shows that the performance differences between the ADRC and MC-ADRC were not very prominent.

For contrast experiment VI, the ADRC algorithm has no MCs, neither α, nor m_b, nor M_{DL}. All of the parameters, including m_b, M_{DL}, and α, were estimated precisely for MC-ADRC. In this test, a disturbance in the adjustment process was also added for pitch angle from 210 seconds to 220 seconds. More specifically, the buoyancy changed fast from 400 mL to 300 mL when the pitch angle changed from –26° to –34°. In that case, the control process encountered was a drastic and strong disturbance. In this experiment, the advantages of MC-ADRC were more apparent than those of ADRC. For both the settling time and the overshoot, the MC-ADRC controller was much better than the ADRC controller.

Spiral Motion Experiments

The algorithm is simulated with the underwater glider in a spiral motion mode. The glider moves from the origin of the inertial coordinate system in a steady spiral glider downward. In this mode, the underwater glider rotation radius was 500 m and the pitch angle was –26°. At 180 seconds, the desired pitch angle became 34°. Figure 7 shows simulation outputs for a steady spiral glider downward in space.

DISCUSSION

Table 3 shows the performance comparisons between ADRC and MC-ADRC through the simulation results in pitch angle and spiral motion control. The symbol M_p represents the overshoot of pitch angle and the symbol t_s denotes the settling time. X, Y, and Z represent the end point of underwater glider trajectory.

Regarding to the pitch angle control experiments in Figure 7, it is obvious that the performances of MC-ADRC are better than those of ADRC in the former four groups of tests (I, II, III, and IV). For the first three tests, the performances of MC-ADRC were not improved significantly relative to ADRC. The reasons are as follows: there was only one parameter (one of three parameters as m_b, M_{DL}, and α) estimated for MC-ADRC and it did not reduce too much burden of estimation for ESO. For results from the experiments I, II, and III, the settling time

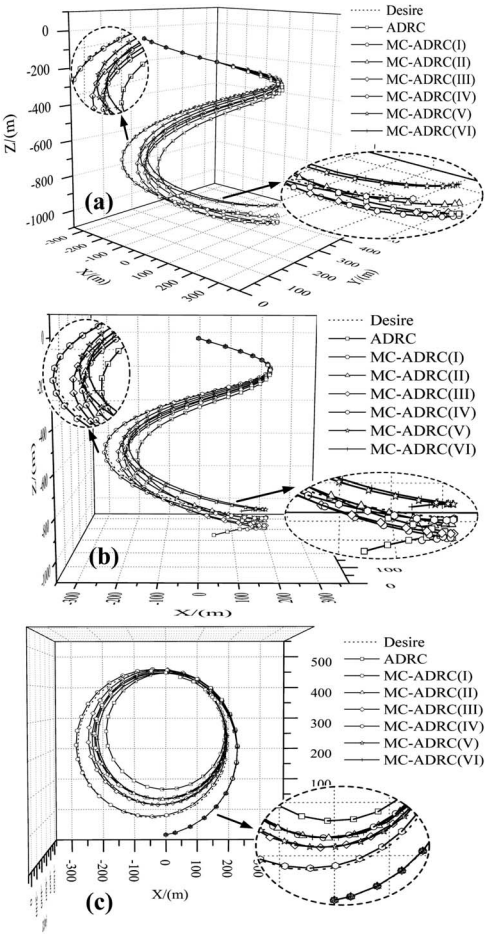

Figure 7. Trajectory control simulation results between ADRC and MC-ADRC in the MATLAB. (a) Three-dimensional motion trajectory. (b) Glider path projected onto XZ plane. (c) Glider path projected onto XY plane.

and overshoot of MC-ADRC were shorter by 43, 75, and 65 seconds and 1.5, 3.2, and 3.7%, respectively, than those of ADRC. Test IV shows that MC-ADRC has an excellent control performance when all of the unknown parameters (m_b, M_{DL}, and α) were estimated precisely. The experiment results show that the settling time and overshoot of the pitch angle were reduced to 2% and 70 seconds respectively. In addition, according to the first four experiments, the more models there are when the controller knows about the system, the better control performances will the controller obtain. Moreover, comparing experiments V and VI, it is very clear that the performances between ADRC and MC-ADRC were not particularly obvious when the disturbance was assuasive. On the one hand, the ESO has a good estimation ability on slow signals. On the other hand, when the disturbance was drastic, the performance differences were great. That means the estimation pressures are burdensome. The ESO was overwhelmed for so many estimation parameters.

Similarly, for the 3D trajectory control experiments, it can be seen from Figure 7 and Table 5 that the control accuracy of the MC-ADRC controllers is significantly higher than that of the ADRC controllers, and the motion trajectory curve of the underwater glider using the MC-ADRC controller was very close to the desired trajectory curve. The desired end point of the underwater glider path was at 187.6, 171.9, and –889.3 m in the x, y, and z axes. However, the underwater glider using ADRC controller glided to 46.6, 435.0, and –1158.0 m. The trajectory of the glider has seriously deviated from the expected trajectory.

In experiments I, II, and III, the parameters α, m_b, and M_{DL} were compensated or estimated in the ADRC controller. The end points of the underwater glider's trajectory were closer to expectations. Experiment IV illustrates that MC-ADRC has an excellent control performance when all of the unknown parameters (m_b, M_{DL}, and α) were estimated. The results illustrate that the glider only deviated 5.6, 0.9, and 1.8 m on three axes, respectively. Obviously, the trajectory of the glider was highly consistent with the expectations. Thus, it is clear that when the controller knows more about the model, it has better control performance. In addition, from experiments V and VI, if the disturbance is fast, the control process would be difficult and the results may deviate from expectations. However, when the disturbance is slowly imposed, the control performance would be improved so that the MC-ADRC controller has more robust ability to control the trajectory of the glider. It is very helpful and important for continuous and accurate observations of the underwater glider.

CONCLUSIONS

This paper presented a MC algorithm based on ADRC for an underwater glider. ADRC was adopted to solve the coupling problem in the pitch angle control loop and ESO was used to estimate the uncertain parameters for the glider. The MC based on ADRC was presented to reduce the estimation burden for the ESO and increase the control precision and response speed. Parameter identification method, parameter estimation method, and a physical sensor were applied to obtain the uncertain parameters for MC.

Simulation results show that the MC has greatly reduced the observation pressure and estimation burden for ESO. More particularly, the more model information the controller has about the system, the better control performance the controller obtains. In the simulation experiments on MATLAB, MC-ADRC reduced overshoot by 3.6% and settling time by 75 seconds for pitch angle compared with traditional ADRC, on average. It guaranteed a precise trajectory of motion. Next, the MC-ADRC algorithm will be applied to the actual underwater glider control system as soon as possible.

ACKNOWLEDGMENTS

This research is financially supported by the Underwater Glider Research Center of Ocean University of China, 863 Plan Acoustic Glider System Development Team (number 2012AA091004), Development of Long-voyage Underwater Glider and Application, and the National Key Research and Development Program of China (number 2016YFC0301102).

LITERATURE CITED

Afande, N.; Arshad, M.R., and Mohd-Mokhtar, R., 2011. Underwater glider modelling and analysis for net buoyancy, depth and pitch angle control. *Ocean Engineering*, 38(16), 1782–1791.

Caffaz, A.; Caiti, A.; Casalino, G., and Gualdesi, L., 2009. Fòlaga: A low cost AUV/glider for coastal environmental sampling. *Underwater Technology,* 28(4), 151–157.

Cao, J.L.; Cao, J.J.; Yao, B.h., and Lian, L., 2015. Dynamics and adaptive fuzzy turning control of an underwater glider. *IEEE Oceans* (Genova, Italy), pp. 1–7.

Carneiro, J.F. and Almeida, F.G., 2018. Model and simulation of the energy retrieved by thermoelectric generators in an underwater glider. *Energy Conversion and Management*, 163, 38–49.

Claus, B.; Bachmayer, R., and Cooney, L., 2012. Analysis and development of a buoyancy-pitch based depth control algorithm for a hybrid underwater glider. *2012 IEEE/OES Autonomous Underwater Vehicles(AUV) Conference* (Southampton, United Kingdom), pp. 1–6.

Eriksen, C.C.; Osse, T.J.; Light, R.D.; Wen, T.; Lehman, T.W.; Sabin, P.L.; Ballard, J.W., and Chiodi, A.M., 2001. Seaglider: A long-range autonomous underwater vehicle for oceanographic research. *IEEE Journal of Oceanic Engineering,* 26(4), 424–436.

Font, D.; Tresanchez, M.; Siegentahler, C.; Teixido, M.; Pallejà, T.; Pradalier, C., and Palacin, J., 2011. Experimental determination of the hydrofoil's angle of attack in the case of a turtle-like autonomous underwater vehicle. *IEEE Oceans* (Santander, Spain), pp. 1–5.

Gao, Z.Q., 2006. Active disturbance rejection control: A paradigm shift in feedback control system design. *Proceedings of the American Control Conference (Minneapolis, USA)*, pp. 2399–2405.

Glenn, S.; Schofield, O.; Kohut, J.; McDonnell, J.; Ludescher, R.D.; Seidel, D.; Aragon, D., and Haskins, C., 2011. The Trans-Atlantic Slocum glider expeditions: A catalyst for undergraduate participation in ocean science and technology. *Marine Technology Society Journal*, 45(1), 52–67.

Graver, G.J., 2005. Underwater gliders: Dynamics, control and design. *Journal of Fluids Engineering*, 127(3), 523–528.

Han, J.Q., 2009. From PID to active disturbance rejection control. *IEEE Transactions on Industrial Electronics*, 56(3), 900–906.

Isa, K. and Arshad, M.R., 2013. Modeling and motion control of a hybrid-driven underwater glider. *Indian Journal of Geo-Marine Sciences*, 42(8), 971–979.

Isa, K. and Arshad, M.R., 2013. Propeller-driven underwater glider modelling and motion control. *International Journal of Imaging & Robotics*, 10(2), 86–104.

Leonard, N.E. and Graver, J.G., 2001. Model-based feedback control of autonomous underwater gliders. *IEEE Journal of Oceanic Engineering*, 26(4), 633–645.

Leonard, N.E.; Paley, D.A.; Lekien, F.; Sepulchre, R.; Fratantoni D.M., and Davis, R.E., 2007. Collective motion, sensor networks, and ocean sampling. *Proceedings of the IEEE*, 95(1), 48–74.

Liu, L.; Xiao, L.; Lan, S.Q., and Liu, T.T., 2018. Using Petrel II glider to analyze underwater noise spectrogram in the South China Sea. *Acoustics Australia*, 46(2), 151–158.

Mahmoudian, N. and Woolsey, C.A., 2009. Underwater glider motion control. *Proceedings of the IEEE Conference on Decision and Control* (Cancun, Mexico), pp. 552–557.

Noh, M.M.; Arshad, M.R., and Mokhtar, R.M., 2011. Depth and pitch control of USM underwater glider: Performance comparison PID vs. LQR. *Indian Journal of Geo-Marine Sciences*, 40(2), 200–206.

Rivera, D.E.; Morari, M., and Skogestad, S., 1986. Internal model control. 4. PID controller design. *Industrial & Engineering Chemistry Process Design and Development*, 25(1), 252–265.

Schofield, O.; Kohut, J.; Aragon, D.; Creed, L.; Graver, J.; Haldeman, C.; Kerfoot, J.; Roarty, H.; Jones, C.; Webb, D., and Glenn, S., 2007. Slocum gliders: Robust and ready. *Journal of Field Robotics*, 24(6), 473–485.

Sherman, J.; Davis, R.; Owens, W.B., and Valdes, J., 2001. The autonomous underwater glider "Spray". *IEEE Journal of Oceanic Engineering*, 26(4), 437–446.

Shih, R.; Horng, M.F.; Pan, T.S.; Pan, J.S., and Chen, C.Y., 2016. A genetic-based effective approach to path-planning of autonomous underwater glider with upstream-current avoidance in variable oceans. *Soft Computing*, 21(18), 1–18.

Song, D.L.; Guo, T.T.; Sun, W.C.; Jiang, Q.L., and Yang, H., 2018. Using an active disturbance rejection decoupling control algorithm to improve operational performance for underwater glider applications. *Journal of Coastal Research*, 34(3), 724–737.

Su, Y.X.; Duan, B.Y.; Zheng, C.H.; Zhang, Y.F.; Chen, G.D., and Mi, J.W., 2004. Disturbance-rejection high-precision motion control of a Stewart platform. *IEEE Transactions on Control Systems Technology,* 12(3), 364–374.

Sun, D., 2007. Comments on active disturbance rejection control. *IEEE Transactions on Industrial Electronics*, 54(6), 3428–3429.

Tchilian, R.S.; Rafikova, E.; Gafurov, S., and Rafikov, M., 2017. Optimal control of an underwater glider vehicle. *Procedia Engineering,* 176, 732–740.

Wang, S.X.; Sun, X.J.; Wu, J.G.; Wang, X.M., and Zhang, H.W., 2010. Motion characteristic analysis of a hybrid-driven underwater glider. *IEEE Oceans* (Sydney, New South Wales, Australia), pp. 1–9.

Wilcox, D.C., 2008. Formulation of the k - ω turbulence model revisited. *AIAA Journal*, 46(11), 2823–2838.

Xue, W.C. and Huang, Y., 2014. On performance analysis of ADRC for a class of MIMO lower-triangular nonlinear uncertain systems. *ISA Transactions*, 53(4), 955–962.

Yoon, S. and Kim, J., 2017. Trajectory design of underwater gliders for maximum advance speed in finite-depth water. *Journal of Guidance, Control, and Dynamics*, 41(3), 1–8.

Zheng, Q.; Chen, Z., and Gao Z.Q., 2009. A practical approach to disturbance decoupling control. *Control Engineering Practice*, 17(9), 1016–1025.